B cell homeostasis and follicle confines are governed by fibroblastic reticular cells

Published in final edited form as:
Nat Immunol. 2014 October ; 15(10): 973–981. doi:10.1038/ni.2965.

B cell homeostasis and follicle confines are governed by fibroblastic reticular cells

Viviana Cremasco[1,9], **Matthew C. Woodruff**[2,3,9], **Lucas Onder**[4], **Jovana Cupovic**[4], **Janice M. Nieves-Bonilla**[1], **Frank A. Schildberg**[1], **Jonathan Chang**[1,3], **Floriana Cremasco**[1,5], **Christopher J. Harvey**[1], **Kai Wucherpfennig**[1], **Burkhard Ludewig**[4], **Michael C. Carroll**[2,6], and **Shannon J. Turley**[1,7,8]

[1]Department of Cancer Immunology and AIDS, Dana Farber Cancer Institute, Boston, Massachusetts, 02115 [2]Program in Cellular and Molecular Medicine, Children's Hospital, Boston, Massachusetts, 02115 [3]Division of Medical Sciences, Harvard Medical School, Boston, MA 02115, USA [4]Institute of Immunobiology, Kantonal Hospital St. Gallen, 9007 St. Gallen, Switzerland [5]Department of Pharmacology, University of Milan, via Balzaretti 9, 20133 Milan, Italy [6]Department of Pediatrics, Harvard Medical School, Boston, MA 02115, USA [7]Department of Microbiology and Immunobiology, Harvard Medical School, Boston, MA 02115, USA

Abstract

Fibroblastic reticular cells (FRCs) are known to inhabit T cell-rich areas of lymphoid organs where they function to coordinate T cell and dendritic cell interactions. However, *in vivo* manipulation of FRCs has been limited by a dearth of genetic tools targeting this lineage. Here, using a mouse model to conditionally ablate FRCs, we demonstrate their indispensable role in anti-viral T cell responses. Unexpectedly, FRC loss also attenuated humoral immunity due to impaired B cell viability and follicular organization. Follicle-resident FRCs established a favorable niche for B lymphocytes via production of the cytokine BAFF. Thus, our study indicates that adaptive immunity requires an intact FRC network and illuminates a subset of FRCs that controls B cell homeostasis and follicle identity.

Secondary lymphoid organs are essential sites for the induction of adaptive immune responses. One of their most remarkable features is the segregation of B and T cells into discrete domains comprising structural and functional units for optimal immune cell activation[1, 2]. These specialized environments are inhabited by different subsets of mesenchymal stromal cells, which are commonly viewed as serving scaffolding function for

Correspondence should be addressed to S.J.T. (turley.shannon@gene.com) or M.C.C. (michael.carroll@childrens.harvard.edu), Shannon J. Turley, Ph.D., Tel: 650-225-2790, Fax: 650-742-1580. Michael C. Carroll, Ph.D., Tel: 617-713-8700, Fax: 617-713-8702.
[8]Present address: Genentech, 1 DNA Way, South San Francisco, California, 94080.
[9]These authors contributed equally to this work.

AUTHOR CONTRIBUTIONS

V.C. and M.C.W. designed and performed experiments and analyzed results; J.M.N.-B., F.A.S., F.C., J. Cu., L.O., J. Ch. and C.J.H. performed experiments; B.L. provided *Ccl19*-Cre *mice* and critical input on the manuscript; K.W. provided reagents and critical input on the manuscript; M.C.C. and S.J.T. designed and supervised the study. V.C. and S.J.T. wrote the manuscript.

COMPETING FINANCIAL INTERESTS

The authors declare no competing financial interests.

T and B lymphocytes and dendritic cells. Current dogma holds that fibroblastic reticular cells (FRCs) within the paracortical region coordinate T cell responses whereas follicular dendritic cells (FDCs) within the cortex support B cell responses. However, a precise understanding of how the stromal network of lymphoid organs controls adaptive immunity has been beyond our reach due to limitations in the technology for targeting each of the mesenchymal cell populations.

The T cell paracortical region of the lymph node is delineated by FRCs, the most abundant population of non-hematopoietic or stromal cells in this organ. Typified by expression of the glycoprotein podoplanin (PDPN), and molecules such as CD140α and CD140β, FRCs construct an elaborate conduit network that allows small molecules to rapidly flow from upstream tissues deep into the parenchyma of lymph nodes[3–5]. Expression of CCL19 and CCL21 by FRCs, in addition to other adhesion molecules, facilitates chemokine receptor CCR7-dependent homing of naive T cells and provides essential guidance cues to dendritic cells that migrate from non-lymphoid tissues into the lymph node paracortex[6–8]. Additionally, interleukin 7 (IL-7) production by FRCs is thought to be essential for preservation of the peripheral T cell pool under homeostatic conditions[9]. More recently, FRCs have also been found to control the extent of proliferation of newly activated T cells through regulated release of nitric oxide[10–12].

The two stromal cell populations commonly characterized within the lymph node cortex include FDCs and marginal reticular cells (MRCs). FDCs are characterized by localization within B cell follicles, expression of the complement receptors CR1 and CR2 (CD21 and CD35) and the follicular dendritic cell marker 1 (FDCM1), and the ability to display opsonized antigens to B cells. Expression of B cell trophic factors, namely the chemokine CXCL13 and the pro-survival factor BAFF (also known as BlyS, TALL-1, TNFSF13B, TNFSF20), is often attributed to FDCs, implicating these cells in shepherding B cells to follicles, supporting B cell survival and coordinating the germinal center reaction[13–16]. Previous work employing a system to ablate FDCs provided definitive evidence that, while this stromal subset is critical for germinal center responses, it plays only a minor role in B cell homeostasis within resting lymph nodes[17]. Likewise, loss of FDCs was not mirrored by a decrease in *Tnfsf13b*, hereafter referred to as *Baff*, transcript abundance, pointing to the presence of an alternative source. These observations have led some investigators to postulate that MRCs, which reside in close juxtaposition to the subcapsular sinus (SCS) of lymph nodes[18], serve these functions, but data supporting this hypothesis are not yet available. Thus, the cell population supporting B cell homeostasis within primary follicles has remained enigmatic.

We have developed and experimentally validated an inducible mouse model (*Ccl19*-Cre x *Rosa26*-diphtheria toxin receptor (iDTR) mice) for conditional ablation of FRCs *in vivo*. In these mice, administration of diphtheria toxin (DTxn) caused a rapid and extensive depletion of FRCs, while sparing other stromal cell populations. Our data demonstrate that FRC ablation led to marked alterations in T cell homeostasis and compartmentalization, with profound consequences in the activation, expansion and effector function of viral antigen-specific T lymphocytes. Unexpectedly, loss of FRCs also led to significantly reduced B cell viability and altered follicular organization, followed by marked impairment in humoral

immunity to T-dependent and T-independent viral antigens. Mechanistically, we determined that a subset of FRCs residing within lymphoid follicles establishes a favorable niche for B lymphocytes via production of BAFF.

Collectively, these results demonstrate that FRCs are required for the generation of virus-specific T cell responses within lymphoid organs. Additionally, our study broadens the current paradigm of FRCs solely supporting T cell immunity, and highlights an essential role for FRCs in directly controlling B cell homeostasis, distribution and activation.

Results

In vivo genetic targeting and selective ablation of FRCs

Manipulation of FRCs *in vivo* has thus far been limited by a lack of specific genetic models targeting this population of stromal cells. A transgenic Cre mouse line that permits targeting of FRCs, in which expression of Cre recombinase is directed by the *Ccl19* promoter[19], was only recently generated. By crossing the transgenic *Ccl19*-Cre line to *Rosa26*-enhanced yellow fluorescent protein (EYFP) mice, we have generated *Ccl19*-Cre x *Rosa26*-EYFP reporter mice, in which EYFP expression is achieved following Cre-mediated excision of a *lox*P-flanked transcriptional "stop" sequence (Supplementary Fig. 1a). Confocal laser scanning microscopy of lymph nodes from *Ccl19*-Cre x *Rosa26*-EYFP mice revealed expression of the transgene in the T cell zone, thereby supporting efficient excision of floxed loci in the expected location (Fig. 1a,b). Flow cytometric analysis demonstrated EYFP expression in FRCs, identified as non-hematopoietic cells expressing the glycoprotein podoplanin (PDPN) and negative for the endothelial marker CD31 and the cell adhesion molecule MadCAM-1 ($CD45^-PDPN^+CD31^-MadCAM^-$) (Fig. 1c and Supplementary Fig. 1b). EYFP expression was not detected in other lymph node stromal cells including lymphatic endothelial cells (LECs, $CD45^-PDPN^+CD31^+$), blood endothelial cells (BECs, $CD45^-PDPN^-CD31^+$) or integrin α_7-expressing pericytes (IAPs, CD45–$PDPN^-CD31^-$) (Fig. 1c), thereby confirming specificity of the *Ccl19* promoter. Despite the recent reports suggesting a close developmental relationship between FRCs and MRCs[20] ($CD45^-PDPN^+CD31^-MadCAM^+$), MRCs did not appear to be targeted with *Ccl19*-directed recombinase, as demonstrated by the absence of EYFP expression in MadCAM-1^+ cells lining the subcapsular sinus by flow cytometry and confocal microscopic analysis (Fig. 1c–e).

To generate a mouse model that enables selective depletion of FRCs, mice harboring the gene encoding DTR downstream of a floxed transcriptional stop element in the ubiquitously expressed *Rosa26* locus[21] were crossed to *Ccl19*-Cre mice (Supplementary Fig. 1c). In these mice, cells with an active *Ccl19* promoter (FRCs) express the simian DTR, and are selectively vulnerable to toxin-induced apoptosis when exposed to DTxn. A single injection of DTxn into these mice was sufficient to achieve rapid and extensive ablation of FRCs from lymph nodes. FRCs were lost as early as 24 h following DTxn administration (Fig. 2a–c) and deletion was specific, as we did not detect changes in cellularity of other lymph node stromal populations, including LECs, BECs and IAPs (Fig. 2d). Consistent with FRCs being the predominant source of the chemokine CCL19 (refs. [8,9]), its expression in lymph nodes was abrogated after FRC ablation, whereas expression of genes shared with other cells, such

as *Ccl21* (ref. [8]), was only partially reduced (Fig. 2e,f). As such, we were able to detect MadCAM-1^{+}RANK-L^{+} cells along the lymph node subcapsular sinus of FRC-ablated mice (Fig. 2g and Supplementary Fig. 1d), confirming a lack of *Ccl19* promoter activity in MRCs. In line with this finding, *Rank-l* transcript encoded by *Tnfsf11*, which is shared by MRCs and FRCs[8,18], was only partially reduced in total lymph node mRNA preparation after FRC ablation (Supplementary Fig. 1e), despite complete abrogation of *Ccl19* (Fig. 2e).

Despite FRCs comprising a minute cellular compartment (~0.5% of total lymph node cells)[22], their ablation resulted in marked alterations in lymph nodes, with significant reductions in organ size, weight and cellularity (Fig. 3a,b and data not shown). However, these effects were not symptomatic of a global collapse of lymph node architecture, as FRC ablation perturbed neither the integrity nor the permeability of the conduit network (Fig. 3c). DTxn administration was not associated with systemic toxicity, and it did not lead to weight loss or extra-nodal pathology (Supplementary Fig. 2a and data not shown). Furthermore, we did not observe accumulation of either neutrophils (CD11b^{+}Gr1^{high}) or monocytes (CD11b^{+}Gr1$^{-/lo}$), or increased expression of inflammatory cytokines, ruling out extraneous inflammation secondary to FRC ablation (Supplementary Fig. 2b,c). Collectively, these data suggest that the *Ccl19*-Cre mouse system allows for specific ablation of FRCs *in vivo*.

Ablation of FRCs impairs anti-viral T cell responses

Confocal laser scanning microscopy of DTxn-treated mice confirmed disappearance of FRCs from the T cell zone parenchyma, and revealed aberrant localization of T lymphocytes within cortical regions (Fig. 4a). Notably, we also observed a global reduction of T cell numbers in lymph nodes (Fig. 4b) with both CD4^{+} and CD8^{+} T cells equally affected by loss of FRCs (Supplementary Fig. 3a,b). Moreover, expression of the T cell survival factor *Il-7* was also reduced in lymph nodes from FRC-ablated mice, suggesting that diminished T cell viability may compound the reduction in T cell numbers (Fig. 4c). To assess the impact of FRC ablation in adaptive T cell responses, *Ccl19*-Cre x iDTR mice were immunized with a replication-incompetent influenza A virus expressing the OT-II ovalbumin peptide, and the generation of antigen-specific T effector cells was monitored (Supplementary Fig. 3c,d). Loss of FRCs resulted in diminished priming of antigen-specific T cells (Fig. 4d,e), as well as reduced activation and proliferation (Fig. 4f–h). Furthermore, deterioration of anti-viral T cell responses was observed in a coronavirus-based vector system[23], in which we monitored the generation and effector function of exogenously transferred TCR transgenic CD8^{+} T cells specific for the viral spike protein prior to immunization[24] (Supplementary Fig. 3e). Strikingly, generation of the virus-specific T cell response was also profoundly disrupted, with reduced numbers of antigen-specific CD8^{+} T cells and defective interferon-γ production in FRC-ablated mice (Fig. 4i,j). Altogether, our data demonstrate a critical role for FRCs in T cell homeostasis, positioning and activation.

FRC ablation is detrimental to B cells

Unexpectedly, we also observed a substantial reduction in lymph node B cells following DTxn administration (Fig. 5a,b). Structural alterations in the lymph node cortex were also observed, with reduced follicle size (Fig. 5c) and a loss of follicle boundaries (Fig. 5d). Ultimately, this resulted in an unfurling of the B cell zone with mixing of B and T

lymphocytes throughout the cortex (Fig. 5d). Notably, no *Ccl19* promoter activity or intrinsic toxicity of DTxn in B lymphocytes was detected, suggesting a physiologic relationship between B cell homeostasis and the presence of FRCs (Supplementary Fig. 3f,g).

To determine the functional consequences of the aberrant follicular architecture and decreased B cell numbers, we assessed the ability of FRC-ablated mice to mount a humoral response to influenza A virus. Immunization with UV-inactivated influenza virus resulted in a disorganized accumulation of B cells in the ensuing germinal center response (Fig. 5e), as well as a significant reduction in influenza-specific IgM (T-independent[25]) and IgG2b (T-dependent) antibody production (Fig. 5f).

The detrimental effect of FRC ablation on B cells was not restricted to lymph nodes. In splenic white pulp, where the *Ccl19* promoter is active in both FRCs and $CD31^{-}PDPN^{-}$ (DN) cells ([19] and Supplementary Fig. 4a), DTxn administration efficiently targeted $EYFP^{+}$ stroma (Supplementary Fig. 4b,c), with a significant decrease in FRCs and DN cells (Supplementary Fig. 4d,e). FRC ablation had no effect on splenic weight or cellularity (Supplementary Fig. 4f,g) but markedly altered white pulp architecture (Supplementary Fig. 4h). B cell numbers were also reduced in the spleen (Supplementary Fig. 4i), although to a lesser extent than in lymph nodes (Supplementary Fig. 4j). Functionally, the effects observed in the spleen impinged on marginal zone humoral responses, with a significant decrease in IgM production upon TNP-ficoll immunization (Supplementary Fig. 4k). As *Ccl19* promoter activity was also reported in Peyer's patches ([19] and Supplementary Fig. 5a), we investigated the fate of Peyer's patches following FRC ablation. Systemic DTxn administration evoked less severe effects in Peyer's patches, with milder reductions in FRC and B cell numbers (Supplementary Fig. 5b,c). Similarly, no major anatomical alterations were observed, with the exception of a paucity of T cell clusters in interfollicular regions (Supplementary Fig. 5d). Together, these observations pointed to an unanticipated regulation of B cell homeostasis by FRCs, and suggest that damage to the FRC network has deleterious consequences on the cellular circuitries that underpin humoral responses.

Lymph node FRCs support homing and survival of B cells

Given the reported role for FRCs in regulating immune cell trafficking[6,7,9,26], we hypothesized that the decrease in B cell numbers after FRC ablation could stem from impaired lymphocyte homing to lymph nodes. To test this hypothesis, congenic CFSE-labeled B cells were adoptively transferred into DTxn-treated *Ccl19*-Cre x iDTR mice, and enumerated within lymph nodes 90 min and 24 h later by flow cytometry. Donor B cell numbers were markedly reduced in lymph nodes of FRC-ablated mice at both time points (Supplementary Fig. 6a). B cell homing to lymph nodes depends on CCL19 and CXCL12 (ref. [27]), and *Cxcl12* expression in FRCs has been previously documented[8]. Indeed, *Cxcl12* expression was significantly reduced in FRC-ablated mice (Supplementary Fig. 6b), and FRCs were sufficient to evoke B cell chemotaxis *in vitro* (Supplementary Fig. 6c), suggesting that FRCs recruit B cells, possibly via CXCL12 and CCL19. Importantly, blockade of lymphocyte ingress (via treatment with a CD62L blocking antibody) was not sufficient to significantly perturb B cell numbers in the first 24 h after treatment

(Supplementary Fig. 6d), in contrast to the rapid B cell loss observed in FRC-ablated mice (Fig. 5a,b). Additionally, preventing lymphocyte egress from lymph nodes with a sphingosine 1-phosphate receptor antagonist, FTY720, did not completely restore B cell numbers following FRC ablation (Supplementary Fig. 6e). Altogether, these data suggest that while B cell entry requires an intact FRC network, impaired B cell trafficking can only account for part of the reduction in B cell numbers following FRC ablation. This consideration prompted us to investigate the possibility that FRCs may regulate additional aspects of B cell homeostasis. Consistent with this hypothesis, B cell loss in FRC-ablated mice coincided with a significant increase in propidium iodide-positive B cells (Fig. 6a,b) implicating FRCs in promoting B cell survival.

FRC ablation impairs BAFF production *in vivo*

Most efforts to characterize FRCs have thus far focused on their roles in supporting T cell homeostasis, migration and activation. However, a discrete population of FRCs is also found in and around follicles (B cell zone FRCs, Fig. 6c), and we reasoned that such a locale could position FRCs to directly interact with and influence B cells. This observation, together with the decreased B cell survival observed in FRC-ablated mice, led us to hypothesize that FRCs may provide critical survival factors for naive B cells. In this context, BAFF plays a critical role in survival of mature B cells[28,29]. The key source of BAFF in secondary lymphoid organs was previously identified as a radiation resistant cell[30], with FDCs often considered the sole BAFF-producing stromal cell[31]. Thus, we reasoned that the phenotypes observed in FRC-ablated mice may be secondary to a reduction in FDCs. To test if FDCs were directly targeted in our system, we ascertained whether the *Ccl19* promoter was active in FDCs *in situ* by fluorescence imaging in *Ccl19*-Cre x *Rosa26*-EYFP mice. As depicted by FDCM1 and CXCL13 staining, EYFP was absent in the majority of FDCs in steady state lymph nodes (Fig. 6d). Less EYFP staining was detected in a small number of FDCM1$^+$ processes (Fig. 6d), possibly due to the tight interconnections that exist between FRCs and FDCs in follicles[4,32]. Additionally, to assess the status of FDCs in FRC-ablated mice, we performed quantitative microscopic analysis of lymph nodes at different time points after DTxn administration. Our data demonstrated that FDCs are present 24 h after DTxn administration (Fig. 6e and quantified in Fig. 6f), despite profound loss of FRCs (Fig. 2c). Furthermore, FDCs remained functionally competent at this time point, as demonstrated by their ability to correctly display exogenous immune complexes (Supplementary Fig. 7a). Prolonged DTxn exposure led to a progressive reduction in FDC volume, as depicted by a decrease in FDCM1 integrated intensity (Fig. 6e,f) and decreased CD35 staining as well (data not shown). Notably, contraction of the FDC network appeared to be transient and was followed by reappearance of FDCM1$^+$ cells 3 days after FRC ablation (Fig. 6e,f). Furthermore, direct comparison of FRC and FDC ablation revealed that loss of FRCs rapidly abrogated *Baff* expression *in vivo* while depletion of FDCs did not (Fig. 6g). Together these results point to a previously unrecognized regulatory role for FRCs in maintaining BAFF amounts and B cell viability. Accordingly, the large decrease in B cell numbers was only observed in FRC-ablated mice but not in FDC-ablated animals (Fig. 6h). Notably, FRC ablation perturbed *Baff* expression without perturbing expression of the closely related factor *April* encoded by *Tnfsf13* (Fig. 6i,j). Moreover, impaired *Baff* mRNA expression in FRC-ablated mice was mirrored by a similar abrogation in BAFF protein abundance, as assessed by confocal

microscopic analysis of lymph node sections (Fig. 6k). Interestingly, concentrations of BAFF protein in serum were unperturbed in FRC-ablated mice (Supplementary Fig. 7b), indicating that FRC loss influences local BAFF production rather than perturbing a systemic reservoir. Furthermore, by injecting carefully titrated DTxn in the footpad, we were able to achieve anatomically restricted FRC ablation, and consequently B cell loss, only in the draining popliteal lymph nodes, without disrupting distal lymph nodes (Supplementary Fig. 7c,d). Thus, the functional consequences of FRC depletion on B cell homeostasis are primarily mediated by a local effect in the organ where the ablation occurs.

B cell zone FRCs constitute a chief source of BAFF

The data shown so far suggest that FRCs may directly promote B cell survival by serving as a non-redundant source of BAFF, in agreement with previous studies demonstrating *Baff* mRNA expression in highly purified FRCs[8]. Confocal microscopic *in situ* analysis of B cell zone FRCs revealed that these cells are indeed capable of producing BAFF protein (Fig. 7a). In line with this finding, BAFF production was also observed by flow cytometry in a discrete fraction of freshly isolated FRCs (Fig. 7b). Notably, BAFF was rapidly cleaved from the cell surface in a protease-dependent manner, similar to other molecules belonging to the TNF superfamily (Supplementary Fig. 7e). Importantly, $BAFF^+$ cells were characterized by expression of several FRC canonical genes encoding PDPN, α-smooth muscle actin (αSMA), CD44, Cadherin-11, CD140α and CD140β, VCAM, and fibroblast-activation protein (FAP) (Fig. 7c), supporting that these cells are nearly identical to FRCs. Thus, our data suggest that FRCs positioned in follicular regions contribute to B cell homeostasis by providing the pro-survival factor BAFF. To directly test the aforementioned hypothesis, we cultured B cells in the presence or absence of FRCs and measured B cell viability using propidium iodide staining by flow cytometry. Remarkably, B cells exhibited significantly enhanced viability when cultured in the presence of FRCs compared with B cells cultured alone (Fig. 7d). The elevated number of propidium iodide-negative $B220^+$ cells in cultures with FRCs could not be accounted for by proliferation (Supplementary Fig. 7f). To ascertain whether the survival advantage conferred by FRCs was due to a soluble factor, B cells were cultured with stromal cells in separate compartments of a transwell chamber or with FRC-conditioned medium. In both conditions, B cells exhibited enhanced viability indicating the presence of a soluble pro-survival factor derived from FRCs (Fig. 7e). Next we sought to determine whether the pro-survival factor contributed by FRCs was BAFF. To this end, FRC-conditioned medium was pre-incubated with a BAFF-specific blocking antibody prior to addition to B cells. Strikingly, the enhancement of B cell survival was largely abrogated following BAFF neutralization (Fig. 7f). In sum, our data describe a subset of FRCs delineating the borders of B cell follicles in lymph nodes (B cell zone FRCs) that nurture B cells through the production of BAFF (Supplementary Fig. 8).

Discussion

The absence of genetic tools for targeting FRCs has curbed systematic *in vivo* assessment of their precise function in lymphoid organs. Recent generation of *Ccl19*-Cre mice provided a solution to this technological limitation[19]. In particular, cell type-specific expression of DTR allowed us to test the functional outcomes of disrupting the FRC network in physiological

settings. FRC ablation caused a severe reduction in T cell numbers in resting lymph nodes, and marked impairment in antigen-specific T cell responses. Unexpectedly, FRC ablation was not immediately accompanied by a collapse of the structured conduit system, suggesting that lymph node infrastructure can persist and function for longer periods following damage to stromal cells. Rather, the absence of the cellular source of the reticular network (i.e. FRCs) impinged on T cell dynamics and function. Thus, our study demonstrates that FRCs are essential for optimal T cell immunity but not short-term maintenance of the conduit system.

Using this genetic approach we made the unexpected observation that FRCs support B cell homeostasis and the generation of humoral responses. While most lymph node FRCs reside within the T cell-rich paracortex, some localize in the vicinity of follicular conduits near the subcapsular sinus[4,32]. Our identification of *Ccl19*-Cre^{+} cells in B cell follicles (B cell zone FRCs) confirmed that FRCs span both the inner and outer regions of the lymph node[33]. Unexpectedly, we found that B cell zone FRCs constitute a non-redundant source of BAFF. The source of BAFF in secondary lymphoid organs was previously identified as a radio-resistant cell[30], oft attributed to FDCs. This concept was confounded however by reports that abrogation of LTβR signaling, critical for FDC development and maintenance, did not affect BAFF expression or B cell numbers[34–37]. Further, a *Cd21*-Cre conditional ablation system provided evidence that FDCs are dispensable for BAFF expression and naive B cell survival[17]. Although it cannot be excluded that FDCs contribute to BAFF production and their ablation induces a compensatory up-regulation by other cells, these data pointed to an alternate source of BAFF in resting lymph nodes. Based on our data, we propose that B cell zone FRCs represent this source of BAFF and thereby directly support B cell homeostasis. Disrupted follicular organization in FRC-ablated mice may also contribute to decreased B cell survival, as FRCs in intact lymphoid organs would coordinate migration of naive B cells from high endothelial venules to BAFF-rich follicles. Furthermore, while FRC ablation does not appear to impede lymph transit to and within lymph nodes, it may affect the ability of migratory dendritic cells to deliver tissue-derived antigens to T and B cells, thus contributing to the diminished antibody production observed in *Ccl19*-Cre x iDTR mice. Collectively, our findings indicate that alterations in lymph node stromal composition can have catastrophic consequences on immunological competency, with decreased lymphocyte viability and disorganized spatial organization of T and B cell responses.

Having demonstrated a central role for FRCs in B cell homeostasis and humoral immunity, our findings highlight the pleiotropic nature of FRCs and suggest functional heterogeneity within this cellular compartment, raising the intriguing concept of distinct FRC subsets within defined lymph node regions. In this context, stromal cells are thought to arise from a primordial mesenchyme in the lymph node anlagen, which initially develops into lymphoid tissue organizer (LTo) cells[38]. B and T lymphocyte colonization after birth then promotes the development of conventional stromal subsets. Similar expression patterns of cellular markers between MRCs and LTo cells suggested that MRCs differentiate into FRCs and FDCs and continuously supply additional stromal subsets[18]. If indeed FRCs arise from MRCs in adult lymph nodes, then the *Ccl19* promoter must be silenced in MRCs. Furthermore, our studies indicated that most FDCs were devoid of promoter activity, and should thus be refractory to DTxn-induced apoptosis. A few cell processes from FDCM1^{+}

cells displayed weak positivity for EYFP. However, given the tight association between FRCs and FDCs in follicles[4,32], it remains difficult to discern between bona fide promoter activity in these FDCs, or proximity to EYFP$^+$ FRCs in follicular regions. In this regard, we observed functionally competent FDCs early after DTxn administration, when profound loss of FRCs has already occurred, suggesting that FDCs are not directly targeted in this system. Consequently, reduction of FDCM1 staining at later time points, likely mediated by a contraction or de-differentiation of the FDC network, may arise from a yet unrecognized crosstalk between FRCs and FDCs. Our finding that contraction of the FDC network was transient and rapidly followed by a regeneration phase is of particular interest. One potential explanation is that damage to the FDC network, secondary to FRC loss, may induce MRCs to generate new FDCM1$^+$ cells[39].

As complexity of the cellular constituents of lymph node stroma continues to grow, our understanding of their developmental origins and functional interactions remains incompletely understood. Our results demonstrate heterogeneity within the FRC network and indicate functional specialization of T cell zone FRCs versus B cell zone FRCs. BAFF$^+$ FRCs in follicles share common signatures with canonical FRCs, suggesting that there is some relationship between them. However, they differ in their localization, and BAFF-producing cells are not found in T cell areas. As mesenchymal cells are typically highly flexible in nature depending on the surrounding environment, it is possible that BAFF production by B cell zone FRCs is maintained by microanatomic cues. Several functions associated with T cell immunity have been assigned to FRCs[3–7,9,19,26,40], yet the requirement for these cells in humoral responses has not been addressed. Our finding that B and T cell homeostasis is governed by a common stromal cell expands our understanding of the stromal network and underscores its central role in immunity.

Stromal cells have long been recognized as key structural components of secondary lymphoid organs[41]. More recently, we have come to understand how stromal cells interact with hematopoietic cell populations and influence adaptive immunity[42,43]. A number of pathogens have been reported to affect the stromal network in lymphoid organs of humans, non-human primates, and rodents, and such alterations can be deleterious to host defense and vaccine responsiveness[1,44]. Here, we uncovered the existence of a mesenchymal cell population with FRC characteristics that supports follicle identity and B cell survival through localized production of BAFF. We anticipate that these findings may inform new approaches to boost natural and vaccine-induced humoral immunity and protect against potentially devastating infections.

Online methods

Mice

Ccl19-Cre mice were previously described[19]. *Rosa26*-EYFP (stock number 006148), *Rosa26*-DTR (iDTR, stock number 007900) *Cd21*-Cre (stock number 006368) and OT-II (stock number 004194) were purchased from Jackson Laboratory. TCR-S transgenic mice were recently described[24]. Mice were maintained under specific pathogen-free conditions in accordance with institutional and National Institute of Health guidelines and used at 5–7 weeks of age. Experiments were conducted without blinding using sex and age matched

mice for all *in vivo* experiments. For multiple time-point experiments, mice were randomly assigned to each group. Animal studies were approved by the Research Animal Care committee of Dana-Farber Cancer Institute.

Antibodies

The following antibodies were used: αCD45 (30-F11), αCD31 (390), αPDPN (8.1.1), αMadCAM (MECA-367), αB220 (RA3-6B2), αAlphaSMA (1A4), αThy1 (53-2.1), αCD140α (APA5), αCD140b (APB5), αCD106 (429), αCD11b (M1/70), αCD11c (N418), αGr1 (RB6-8C5), αMHC class II (M5/114.15.2), αCD4 (RM4.5) and αCD8 (RM2206) from Biolegend, αBAFF (121808 from R&D), anti-GFP (A10263 from Life Technologies).

Systemic FRC ablation *in vivo*

Ccl19-Cre mice were bred to *Rosa26*-iDTR to generate *Ccl19*-Cre x iDTR animals. DTR^+Cre^+ mice that express DTR in *Ccl19*$^+$ cells and DTR^+Cre^- control mice were injected i.p. with 8 ng/g DTxn and sacrificed at 12, 24, 48 or 72 h as indicated in figure legends. Ablation efficiency was assessed by flow cytometry at various time points with 80–90% reduction in FRCs ($CD45^-PDPN^+CD31^-$) commonly seen by 72 h.

Local FRC ablation *in vivo*

DTR^+Cre^+ mice that express DTR in *Ccl19*$^+$ cells and DTR^+Cre^- control mice were injected in the footpad with 0.5 ng/g DTxn and sacrificed 72 h later. Local ablation was assessed by comparing FRC ablation in draining (popliteal) and non-draining lymph nodes.

FDC ablation *in vivo*

Cd21-Cre mice were bred to *Rosa26*-iDTR to generate *Cd21*-Cre x iDTR animals. For FDC ablation experiments, 6 week-old, male recipients were irradiated and adoptively transferred with bone marrow from WT C57BL/6 mice. 6 weeks after reconstitution, mice were injected i.p. with 8 ng/g DTxn and sacrificed 24 h later.

Anti-viral T cell-dependent responses

Influenza propagation and isolation was carried out as previously described[25]. 3 days after DTxn administration, mice were adoptively transferred with 5×10^6 CFSE-labeled, purified OT-II transgenic $CD4^+$T cells by tail vein. 24 h later, mice received 20 μl virus suspension (1×10^6 p.f.u.) S.C. into the footpad. Mice were sacrificed 24 h later and flow cytometric analysis was performed on popliteal lymph nodes. Activation and CFSE dilution were determined 60 h after T cell transfer. For the coronavirus experiments, DTxn injection was performed 72 h before adoptive T cell transfer[23]. A total of 2×10^6 TCR-S transgenic $CD8^+$T cells were transferred by intravenous injection and, 12 h after transfer, the mice were subcutaneously injected with 3×10^6 of non-replicating coronaviral particles in both flanks[23]. A second injection of non-replicating coronaviral particles was performed 12 h following the first one. Lymph nodes were analyzed 72 h after the first viral particle injection.

Anti-viral humoral responses

2 days after DTxn administration, mice received 20 μl influenza virus suspension (1×10^6 p.f.u.) subcutaneously into the footpad. 14 days later, popliteal draining lymph nodes were collected, cryopreserved and imaged to determine formation of germinal centers. Additionally, serum was collected to determine the presence of influenza-specific antibodies. ELISA analysis of serum was carried out through immobilization of UV-PR8 on a high binding plate, addition of collected serum, and probing for specific binding of IgM or IgG2b (Sigma) using standard alkaline phosphatase development. For TNP-Ficoll immunization experiments, mice were injected with DTxn and, 2 days later, with TNP-ficoll i.p. (250 μg/mouse). IgM antibody titers were determined at day 8 in the blood.

Anti-CD62L and FTY720 treatments

For CD62L blockade, mice received one single dose of MEL-14 CD62L antibody i.p. (200 μg/mouse, BioXcell). To prevent cell egress, mice were injected with 1 mg/kg FTY720 (Fingolimod, R&D) i.p. and, 4 h later, with DTxn. Mice received an additional dose of FTY720 at 48 h and were sacrificed for analysis at 72 h.

BAFF Serum

Serum was collected from mice 3 days after DTxn administration and stored at −80 °C until processing. Soluble BAFF was measured in the serum samples at a 1:2 dilution using a modified cytometric bead array. BD CBA Functional Beads (BD Biosciences) were activated and coated with immunopure streptavidin (Thermo Scientific) per manufacturer's instructions. For array development, a commercial anti-BAFF ELISA kit (R&D systems, catalog #DY2106-05) was used in an inverted manner. Biotinylated detection antibody was incubated with 30 μl of streptavidin-conjugated bead slurry at 3 μg/ml and subsequently washed three times with PBS containing 3% FBS. Following overnight blocking, serum samples were incubated with anti-BAFF beads in Multiscreen plates (Millipore) for 2 h. Beads were then washed three times with 3% FBS in PBS. ELISA capture antibody was used to detect BAFF bound to beads at a concentration of 4 μg/ml. Following 1 h incubation, beads were washed, followed by incubation with goat anti-rat Alexa 546 antibody (Molecular Probes) for 1 h. Beads were washed three times with 3% FBS in PBS followed by an additional four washes in PBS alone. Fluorescence was detected on a BD FACSAriaIIIu, and data were analyzed using FlowJo software.

Enzymatic digestion of lymphoid organs

For flow cytometric analysis or cell culture of lymph node stromal cells, skin-draining lymph nodes from individual mice were dissected and incubated at 37 °C in RPMI containing 0.1 mg/ml Dnase I (Invitrogen), 0.2 mg/ml Collagenase P (Roche) and 0.8 mg/ml Dispase (Roche) for 50–60 min[22]. Cells were collected in PBS containing 2% FBS and 5 mM EDTA every 15–20 min, replacing the digestion medium with new one. Digestion of spleens was performed similarly, and red blood cells were lysed with ACK buffer before analysis by flow cytometry. Peyer's patches were collected and washed in 2 mM EDTA and 1 mM DTT in PBS to remove the epithelium before enzymatic digestion.

FRC culture *in vitro*

Single cell suspensions from pooled skin-draining lymph nodes were enriched for MadCAM-1$^-$ cells using a biotinylated MadCAM-1-specific antibody and anti-biotin microbeads (Miltenyi). Cells were counted and plated at a density of 5×10^5 cells/cm^2 in αMEM supplemented with 10% FBS, 1% penicillin/streptomycin and 1% glutamine. Non-adherent cells were removed after 24 h. After 5 days, primary cultures (FRCs and LECs primarily) were harvested and MACS-purified for CD45$^-$CD31$^-$ cells (FRCs).

FRC-B cell cocultures

FRCs were purified from primary lymph node cultures (see above) and seeded at a concentration of 2.5×10^5 cells/ml in complete αMEM medium. Freshly purified lymph node B cells (B220 negative selection kit, Miltenyi) were overlaid on top of the FRC layer, at a ratio of 1 FRC : 5 B cells. In some experiments, FRCs were grown on the bottom of a transwell system chamber and B cells were added to the top of the insert. Alternatively, B cells were cultured in FRC-conditioned medium (supernatant from purified FRCs collected 5 days after seeding).

BAFF flow cytometry and protease inhibition

Lymph nodes were enzymatically digested and single cell suspensions were stained in flow cytometry buffer. FRCs were identified as negative for staining with propidium iodide and CD45$^-$CD31$^-$PDPN$^+$MadCAM$^-$. A BAFF monoclonal antibody or isotype control (both from R&D, BAFF clone 121808) were used. For protease inhibition, cells were treated with Batimastat (25 μM in DMSO, abcam) and Decanoyl-Arg-Val-Lys-Arg-Chloromethylketone (25 μM in DMSO, Bachem).

Immunohistochemistry and confocal microscopy

Isolated tissues were fixed in 4% paraformaldhehyde (PFA) for 2–4 h, and placed in 30% sucrose until saturation. Tissue was embedded in OCT medium (Optimal Cutting Temperature), frozen, and cut into 10–20 μm sections. Sections were immunostained, and imaged using a Leica SP5X laser-scanning confocal microscope. All of the images with EYFP signal were counterstained with a chicken GFP-specific antibody (Life Technologies), followed by FITC-conjugated anti-chicken antibody.

PE immune complexes deposition

PE-IC uptake by FDCs was assessed by standard confocal microscopy. 18 h following FRC ablation, mice were passively immunized with 100 μg rabbit PE monoclonal antibody, followed 6 h later by S.C. footpad injection of 1 μg PE. Popliteal draining lymph nodes were fixed in 4% PFA, cryopreserved, sectioned, and imaged as described above.

Conduit analysis

Mice were injected i.v. with 3 μg CD35 (clone 8C12) antibody conjugated to alexa-568 6–18 h prior to lymph node harvest. Conduit staining was achieved through s.c. injection of FITC-saturated PBS solution (10 μl) into the footpad 4–6 h prior to popliteal lymph node harvest.

FDC quantitation

Popliteal lymph nodes from DTxn-treated mice were isolated and fixed in 4% PFA. Lymph nodes were equilibrated in 30% sucrose and serially sectioned. 4 sections from each individual lymph node were taken at 100 μm increments through the lymph node, and stained for confocal microscopic analysis. Resulting images were analyzed using CellProfiler to identify individual B cell follicles within each section. Fluorescence data was assessed for each follicle, and then integrated such that each lymph node data point represents at least 3 combined sections.

Statistical analysis

Two-tailed, unpaired student's *t*-tests were performed, assuming equal sample variance, using GraphPad Prism. Differences were considered to be statistically significant when $P < 0.05$. For graphs, data are shown as mean +/− SD, unless otherwise indicated. Sample size was not specifically predetermined, but the number of mice used was consistent with prior experience with similar experiments.

Supplementary Material

Refer to Web version on PubMed Central for supplementary material.

Acknowledgments

We thank L. Cameron for technical assistance at the Dana-Farber cancer Institute Confocal Imaging core. Supported by the US National Institutes of Health (5R01 DK074500-08, 2P01AI045757-15, R21 CA182598-01 to S.J.T.; R01 AI039246, P01 AI078897, R37 AI054636 to M.C.C.; and T32 CA 070083-15 to V.C.), Claudia Adams Barr Award for Innovative Cancer Research to S.J.T. and Cancer Research Institute fellowship to V.C., grants from the Vontobel Foundation (Zürich, Switzerland) and the Helmut Horten Foundation (Lugano, Switzerland) to B.L.

References

1. Mueller SN, Germain RN. Stromal cell contributions to the homeostasis and functionality of the immune system. Nat Rev Immunol. 2009; 9:618–629. [PubMed: 19644499]
2. Turley SJ, Fletcher AL, Elpek KG. The stromal and haematopoietic antigen-presenting cells that reside in secondary lymphoid organs. Nat Rev Immunol. 2010; 10:813–825. [PubMed: 21088682]
3. Gretz JE, Norbury CC, Anderson AO, Proudfoot AE, Shaw S. Lymph-borne chemokines and other low molecular weight molecules reach high endothelial venules via specialized conduits while a functional barrier limits access to the lymphocyte microenvironments in lymph node cortex. J Exp Med. 2000; 192:1425–1440. [PubMed: 11085745]
4. Roozendaal R, et al. Conduits mediate transport of low-molecular-weight antigen to lymph node follicles. Immunity. 2009; 30:264–276. [PubMed: 19185517]
5. Sixt M, et al. The conduit system transports soluble antigens from the afferent lymph to resident dendritic cells in the T cell area of the lymph node. Immunity. 2005; 22:19–29. [PubMed: 15664156]
6. Acton SE, et al. Podoplanin-rich stromal networks induce dendritic cell motility via activation of the C-type lectin receptor CLEC-2. Immunity. 2012; 37:276–289. [PubMed: 22884313]
7. Astarita JL, Acton SE, Turley SJ. Podoplanin: emerging functions in development, the immune system, and cancer. Front Immunol. 2012; 3:283. [PubMed: 22988448]
8. Malhotra D, et al. Transcriptional profiling of stroma from inflamed and resting lymph nodes defines immunological hallmarks. Nat Immunol. 2012; 13:499–510. [PubMed: 22466668]
9. Link A, et al. Fibroblastic reticular cells in lymph nodes regulate the homeostasis of naive T cells. Nat Immunol. 2007; 8:1255–1265. [PubMed: 17893676]

10. Khan O, et al. Regulation of T cell priming by lymphoid stroma. PLoS ONE. 2011; 6:e26138. [PubMed: 22110583]
11. Lukacs-Kornek V, et al. Regulated release of nitric oxide by nonhematopoietic stroma controls expansion of the activated T cell pool in lymph nodes. Nat Immunol. 2011; 12:1096–1104. [PubMed: 21926986]
12. Siegert S, et al. Fibroblastic reticular cells from lymph nodes attenuate T cell expansion by producing nitric oxide. PLoS ONE. 2011; 6:e27618. [PubMed: 22110693]
13. Cyster JG. B cell follicles and antigen encounters of the third kind. Nat Immunol. 2010; 11:989–996. [PubMed: 20959804]
14. Cyster JG, et al. Follicular stromal cells and lymphocyte homing to follicles. Immunol Rev. 2000; 176:181–193. [PubMed: 11043777]
15. Roozendaal R, Carroll MC. Complement receptors CD21 and CD35 in humoral immunity. Immunol Rev. 2007; 219:157–166. [PubMed: 17850488]
16. Tew JG, Kosco MH, Burton GF, Szakal AK. Follicular dendritic cells as accessory cells. Immunol Rev. 1990; 117:185–211. [PubMed: 2258191]
17. Wang X, et al. Follicular dendritic cells help establish follicle identity and promote B cell retention in germinal centers. J Exp Med. 2011; 208:2497–2510. [PubMed: 22042977]
18. Katakai T, et al. Organizer-like reticular stromal cell layer common to adult secondary lymphoid organs. J Immunol. 2008; 181:6189–6200. [PubMed: 18941209]
19. Chai Q, et al. Maturation of lymph node fibroblastic reticular cells from myofibroblastic precursors is critical for antiviral immunity. Immunity. 2013; 38:1013–1024. [PubMed: 23623380]
20. Katakai T. Marginal reticular cells: a stromal subset directly descended from the lymphoid tissue organizer. Front Immunol. 2012; 3:200. [PubMed: 22807928]
21. Buch T, et al. A Cre-inducible diphtheria toxin receptor mediates cell lineage ablation after toxin administration. Nat Methods. 2005; 2:419–426. [PubMed: 15908920]
22. Fletcher AL, et al. Reproducible isolation of lymph node stromal cells reveals site-dependent differences in fibroblastic reticular cells. Front Immunol. 2011; 2:35. [PubMed: 22566825]
23. Cervantes-Barragan L, et al. Dendritic cell-specific antigen delivery by coronavirus vaccine vectors induces long-lasting protective antiviral and antitumor immunity. mBio. 2010; 1:4.
24. Cupovic, J. PhD thesis. Eidgenössische Technische Hochschule Zürich; 2014. Low avidity $CD8^+$ T cells in viral infection from neuroinflammation to adoptive T cell therapy.
25. Gonzalez SF, et al. Capture of influenza by medullary dendritic cells via SIGN-R1 is essential for humoral immunity in draining lymph nodes. Nat Immunol. 2010; 11:427–434. [PubMed: 20305659]
26. Chyou S, et al. Fibroblast-type reticular stromal cells regulate the lymph node vasculature. J Immunol. 2008; 181:3887–3896. [PubMed: 18768843]
27. Okada T, et al. Chemokine requirements for B cell entry to lymph nodes and Peyer's patches. J Exp Med. 2002; 196:65–75. [PubMed: 12093871]
28. Mackay F, Browning JL. BAFF: a fundamental survival factor for B cells. Nat Rev Immunol. 2002; 2:465–475. [PubMed: 12094221]
29. Mackay F, et al. Mice transgenic for BAFF develop lymphocytic disorders along with autoimmune manifestations. J Exp Med. 1999; 190:1697–1710. [PubMed: 10587360]
30. Gorelik L, et al. Normal B cell homeostasis requires B cell activation factor production by radiation-resistant cells. J Exp Med. 2003; 198:937–945. [PubMed: 12975458]
31. Garin A, et al. Toll-like receptor 4 signaling by follicular dendritic cells is pivotal for germinal center onset and affinity maturation. Immunity. 2010; 33:84–95. [PubMed: 20643339]
32. Gonzalez SF, et al. Trafficking of B cell antigen in lymph nodes. Annu Rev Immunol. 2011; 29:215–233. [PubMed: 21219172]
33. Bajenoff M, Germain RN. B-cell follicle development remodels the conduit system and allows soluble antigen delivery to follicular dendritic cells. Blood. 2009; 114:4989–4997. [PubMed: 19713459]
34. Alimzhanov MB, et al. Abnormal development of secondary lymphoid tissues in lymphotoxin beta-deficient mice. Proc Natl Acad Sci USA. 1997; 94:9302–9307. [PubMed: 9256477]

35. Boulianne B, et al. AID-expressing germinal center B cells cluster normally within lymph node follicles in the absence of FDC-M1+ CD35+ follicular dendritic cells but dissipate prematurely. J Immunol. 2013; 191:4521–4530. [PubMed: 24068672]

36. Browning JL, et al. Lymphotoxin-beta receptor signaling is required for the homeostatic control of HEV differentiation and function. Immunity. 2005; 23:539–550. [PubMed: 16286021]

37. Koni PA, et al. Distinct roles in lymphoid organogenesis for lymphotoxins alpha and beta revealed in lymphotoxin beta-deficient mice. Immunity. 1997; 6:491–500. [PubMed: 9133428]

38. Mebius RE. Organogenesis of lymphoid tissues. Nat Rev Immunol. 2003; 3:292–303. [PubMed: 12669020]

39. Jarjour M, et al. Fate mapping reveals origin and dynamics of lymph node follicular dendritic cells. J Exp Med. 2014

40. Yang CY, et al. Trapping of naive lymphocytes triggers rapid growth and remodeling of the fibroblast network in reactive murine lymph nodes. Proc Natl Acad Sci USA. 2014; 111:E109–118. [PubMed: 24367096]

41. Junt T, Scandella E, Ludewig B. Form follows function: lymphoid tissue microarchitecture in antimicrobial immune defence. Nat Rev Immunol. 2008; 8:764–775. [PubMed: 18825130]

42. Koning JJ, Mebius RE. Interdependence of stromal and immune cells for lymph node function. Trends Immunol. 2012; 33:264–270. [PubMed: 22153930]

43. Malhotra D, Fletcher AL, Turley SJ. Stromal and hematopoietic cells in secondary lymphoid organs: partners in immunity. Immunol Rev. 2013; 251:160–176. [PubMed: 23278748]

44. Scandella E, et al. Restoration of lymphoid organ integrity through the interaction of lymphoid tissue-inducer cells with stroma of the T cell zone. Nat Immunol. 2008; 9:667–675. [PubMed: 18425132]

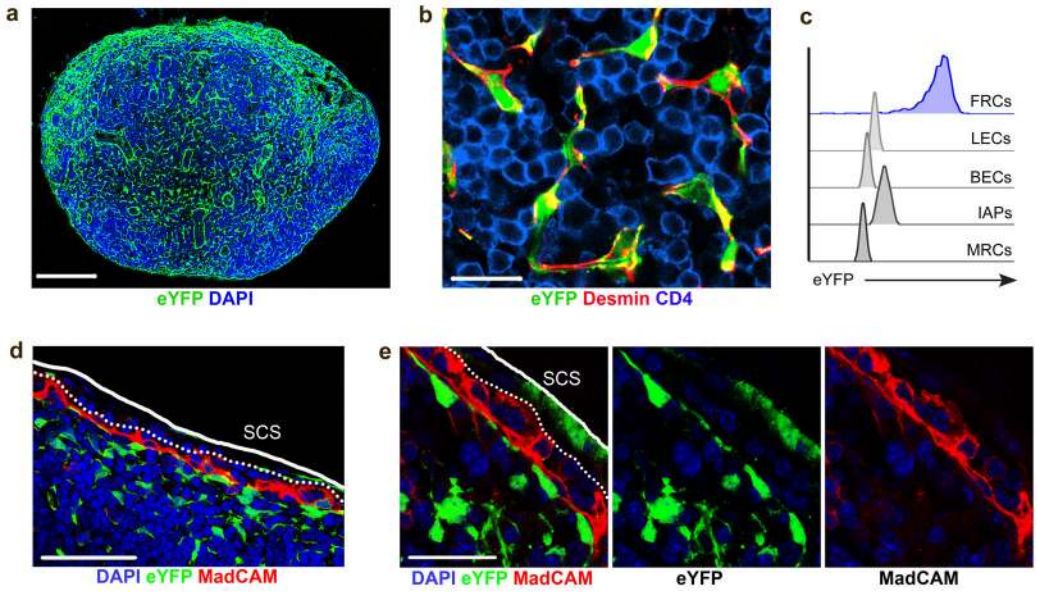

Figure 1. Specific *Ccl19* promoter activity in FRCs

(a) Popliteal lymph node sections from *Ccl19*-Cre x *Rosa26*-EYFP reporter mice were sectioned and stained for GFP and DAPI. Scale bar 200 μm. **(b)** Figure shows higher magnification images of the paracortical area stained for GFP, Desmin and CD4 from mice as in **a**. Scale bar 25 μm (n>3 mice from 3 independent experiments). **(c)** Flow cytometric analysis of freshly isolated stromal cells from *Ccl19*-Cre x *Rosa26*-EYFP mice showing *Ccl19* promoter activity. FRCs, fibroblastic reticular cells; LECs, lymphatic endothelial cells; BECs, blood endothelial cells; IAPs, integrin α_7-expressing pericytes; MRCs, marginal reticular cells (n=3 mice from 2 independent experiments). **(d,e)** Confocal microscopic analysis of lymph nodes from *Ccl19*-Cre x *Rosa26*-EYFP mice stained for DAPI, GFP and MadCAM. SCS, subcapsular sinus. Lines indicate the ceiling and the floor (dotted line) of the subcapsular sinus. Scale bars 50 μm (**d**) and 25 μm (**e**) (n>3 mice from 3 independent experiments).

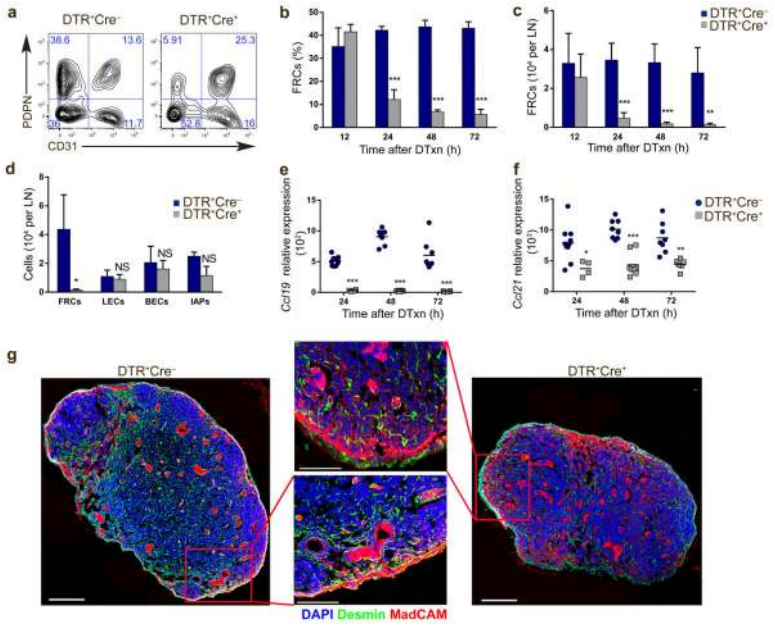

Figure 2. Conditional ablation of FRCs

(a) The FRC ($PDPN^+CD31^-$) compartment was analyzed 24 h after DTxn administration in DTR^+Cre^+ mice that express DTR in *Ccl19+* cells, and in DTR^+Cre^- control mice. Numbers shown in quadrants depict percents. **(b,c)** The effect of DTxn-induced FRC ablation is shown as percent among stromal cells ($CD45^-$) and total number per lymph node. Data are representative of at least three independent experiments (mean+/−sd, *n*=4 mice/group per experiment). **(d)** *Ccl19*-Cre x iDTR mice were injected with DTxn and, 72 h later, lymph nodes were collected, digested and stromal cells enumerated by flow cytometry (FRCs, $CD45^-PDPN^+CD31^-$, LECs, $CD45^-PDPN^+CD31^+$, BECs, $CD45^-PDPN^-CD31^+$, IAPs, $CD45^-PDPN^-CD31^-$). Data are representative of at least three independent experiments (mean+/−sd, n=3 mice/group per experiment). **(e,f)** Following DTxn administration, lymph nodes were collected, lysed in trizol and analyzed for the presence of *Ccl19* or *Ccl21* transcripts. Lines indicate mean. Data are normalized to cyclophillin. Each data point represents one lymph node from an individual mouse (n=4–10 mice/group from 2–3 separate experiments). **(g)** MRCs were identified in lymph nodes from *Ccl19*-Cre x iDTR mice by staining with a MadCAM antibody together with DAPI and anti-Desmin. Scale bars 200 μm and 100 μm for the insets. (n>3 mice from 3 independent experiments). ^{NS} non significant, *p<0.05, **p<0.01, ***p<0.001

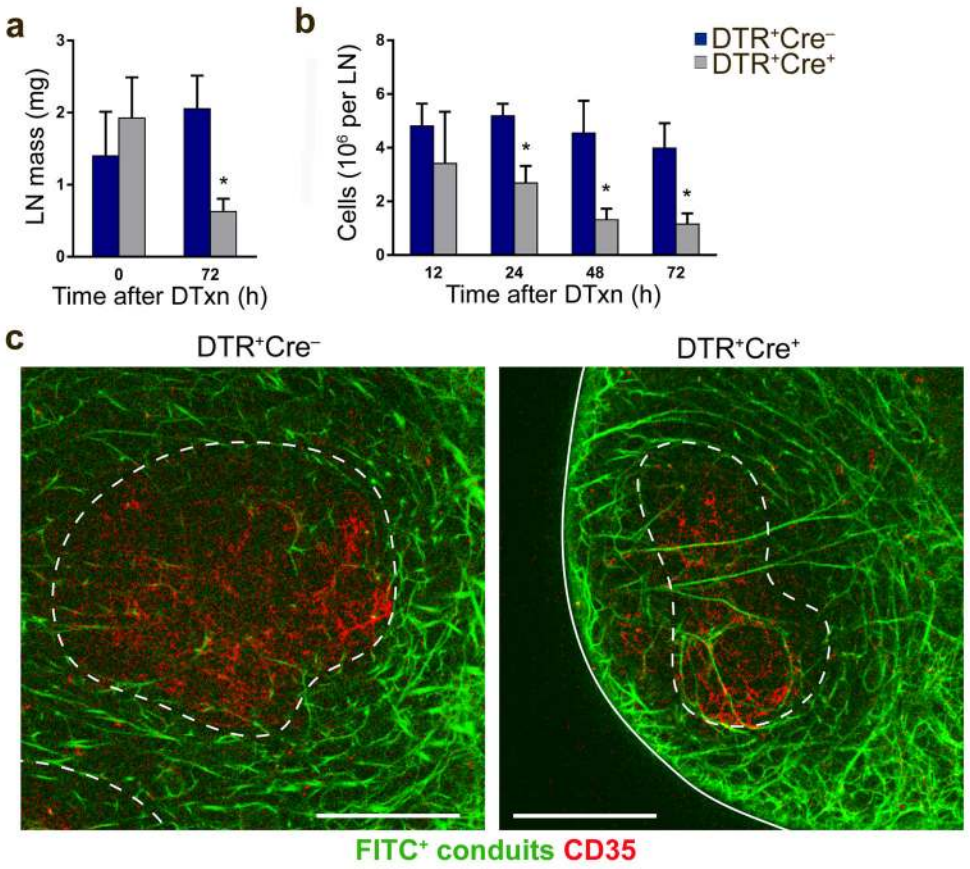

Figure 3. FRC ablation has profound consequences on lymph node cellularity despite preserving conduit functionality

(a,b) Lymph node mass and total cellularity after DTxn administration was determined. Data are representative of at least two independent experiments (mean+/−sd, n=3 mice/group per experiment). **(c)** Representative multiphoton microscopic images of popliteal nodes from *Ccl19*-Cre x iDTR mice depicting FITC-tracer transported into conduits together with staining with a specific CD35 antibody. Scale bars 100 μm (n>3 mice from 2 independent experiments). * p<0.001

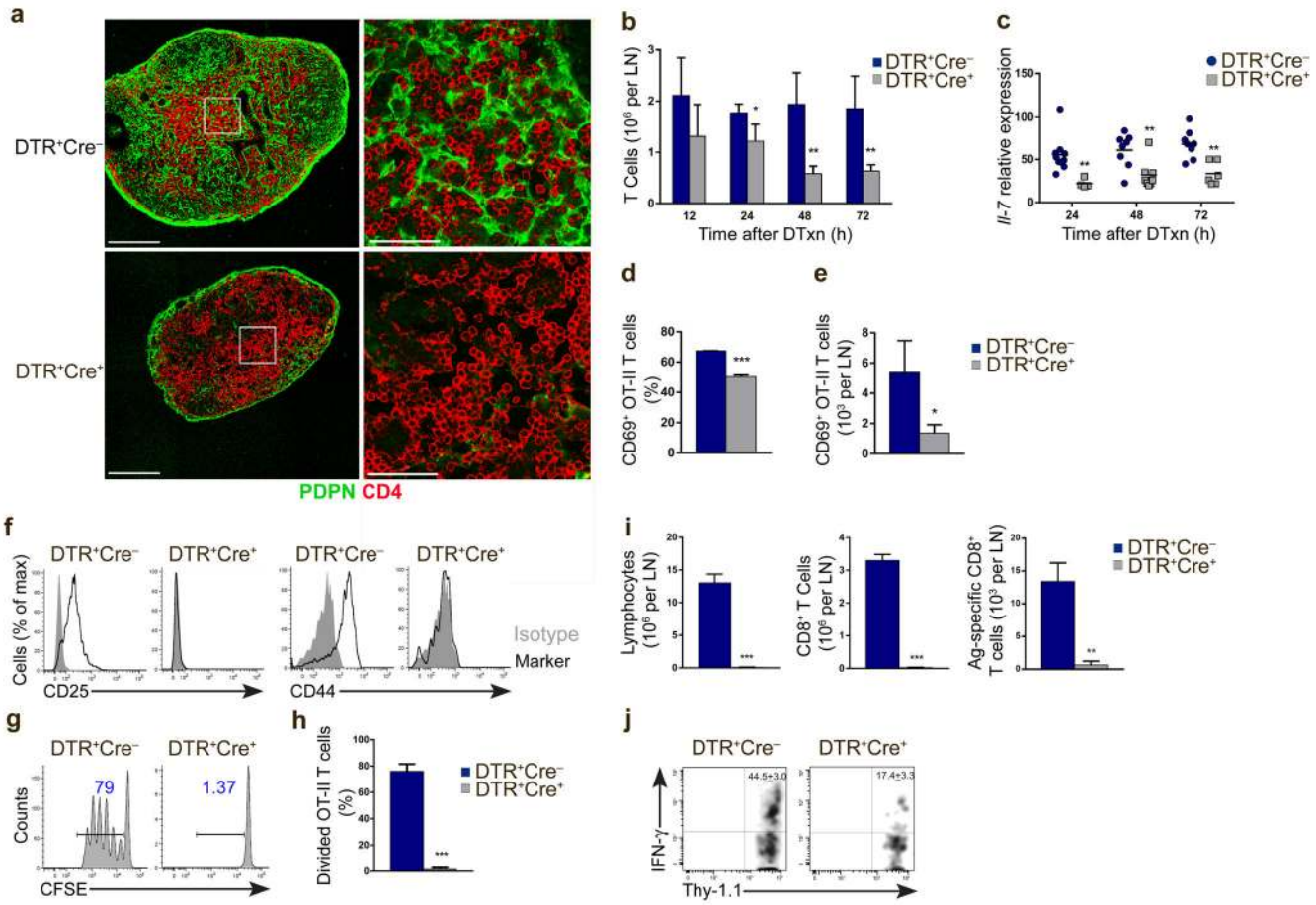

Figure 4. FRC ablation impairs T cell immunity

(a) Confocal microscopy of lymph node sections from *Ccl19*-Cre x iDTR mice stained for CD4 (T cells) and PDPN (FRCs) to depict FRCs in paracortical areas 3 days after DTxn treatment. Scale bars 200 μm (left) and 50 μm (right). (n>3 mice from 3 independent experiments). **(b)** Skin-draining lymph nodes from *Ccl19*-Cre x iDTR mice were collected, and T cells were enumerated using flow cytometric analysis ($CD45^+B220^-CD3^+$). Data are representative of at least three independent experiments (mean+/−sd, n=4 mice/group per experiment). **(c)** Lymph nodes from *Ccl19*-Cre x iDTR mice were collected, lysed in trizol and analyzed for the presence of *Il-7* transcript. Lines indicate mean. Data are normalized to cyclophillin. Each data point represents one lymph node from individual mice (n=4–10 mice/group from 2–3 separate experiments). **(d,e)** Following DTxn treatment, mice were adoptively transferred with CFSE-labeled OT-II T cells. Recipients were immunized with UV-inactivated OVA-expressing influenza virus in the footpad, popliteal nodes were collected 24 h after immunization, and the presence of antigen-specific activated T cells was determined by flow cytometry ($CFSE^+CD3^+CD4^+V\alpha5^+CD69^+$) (n=3 mice/group). **(f)** Flow cytometric analysis of CD25 and CD44 expression by antigen specific T cells 60 h following immunization. **(g,h)** Proliferation of OT-II T cells from mice as in **(f)** was determined as CFSE dilution (n=3 mice/group). **(i)** DTxn-treated mice received $CD8^+$T cells specific for the viral spike protein prior to immunization with non-replicating coronaviral

particles. Numbers of lymphocytes, $CD8^+$T cells and antigen-specific T cells was assessed 72h after virus injection (n=3 mice/group). **(j)** IFNγ production was determined by intracellular staining and flow cytometry (n=3 mice/group). *p<0.05, **p<0.01, ***p<0.001

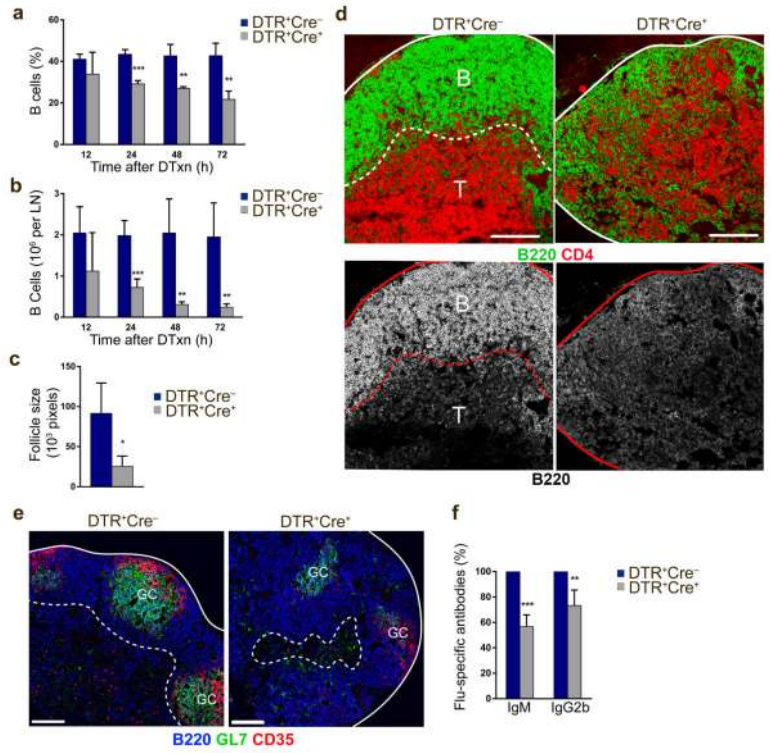

Figure 5. FRC ablation is detrimental to B cells

(a,b) Skin-draining lymph nodes from *Ccl19*-Cre x iDTR mice were collected and B cells numbers were determined by flow cytometric analysis ($CD45^+B220^+CD3^-$). B cell numbers are shown as percent among hematopoietic ($CD45^+$) cells and total numbers per lymph node. Data are representative of at least three independent experiments (mean+/−sd, n=4 mice/group per experiment). **(c,d)** Follicle size (n=3 mice) and architecture (n>3 mice from 3 independent experiments) in lymph node sections from *Ccl19*-Cre x iDTR mice was determined 3 days after DTxn injection by staining with B220 (B cells) and CD4 (T cells). Scale bars 100 μm. **(e)** Popliteal nodes were collected 14 days after influenza immunization and analyzed for the presence of germinal centers. (B220, B cells; GL7, activated B cells; CD35, FDCs.) Scale bars 100 μm. **(f)** T-independent (IgM) and T-dependent (IgG2b) humoral responses were determined by ELISA for the presence of flu-specific serum antibodies. Data are representative of two independent experiments (n=3–5 mice/group per experiment). *p<0.05, **p<0.01, ***p<0.001

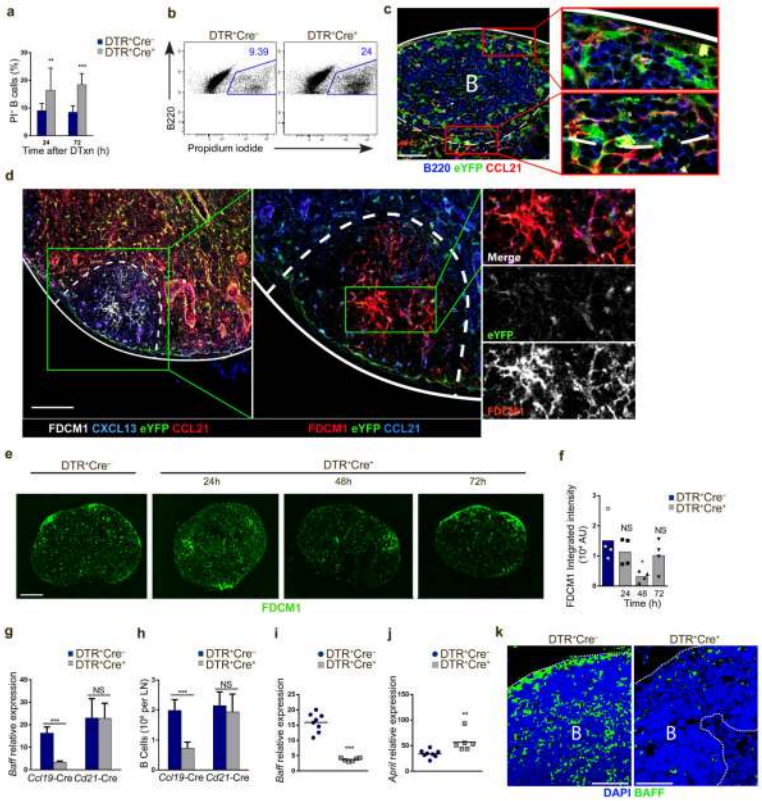

Figure 6. FRC ablation impairs B cell survival

(a,b) B cell viability was assessed by flow cytometric analysis of lymph node single cell suspensions ($CD45^+B220^+PI^+$). Representative dot plots of PI^+ stain in B cells at 72 h are depicted. Data are representative of two independent experiments (n=3–5 mice/group per experiment). **(c)** Confocal images of lymph nodes from *Ccl19*-Cre x *Rosa26-EYFP* mice to depict FRCs in follicular regions. Insets show higher magnifications of the boxed regions. Scale bar 50 μm (n>3 mice from 3 independent experiments). **(d)** Confocal analysis of popliteal lymph nodes from *Ccl19*-Cre x *Rosa26*-EYFP reporter mice stained for FDCM1, CXCL13, GFP and CCL21. Left, chemokine expression is shown; middle, FDCs are identified; right, single channels of the follicle area are provided. Scale bar 100 μm (n>3 mice from 2 independent experiments). **(e)** Confocal analysis of popliteal lymph nodes from *Ccl19*-Cre x iDTR animals 24, 48, or 72 h following DTxn administration. FDCs are identified by FDCM1 stain. Scale bar 200 μm (n>3 mice per group). **(f)** Quantitation of cumulative FDCM1 expression within the follicles of images as in **(e)**. Each point represents a single lymph node from an individual mouse. **(g,h)** Changes in *Baff* expression and B cell numbers were compared between FRC-ablated mice (*Ccl19*-Cre x iDTR) and FDC-ablated mice (*Cd21*-Cre x iDTR, lethally irradiated and reconstituted with WT bone marrow) 24 h after DTxn administration (n=2–4 mice/group). **(i,j)** Three days after DTxn administration, lymph nodes from *Ccl19*-Cre x iDTR were collected, lysed in trizol and analyzed for the presence of *Baff* and *April* transcripts. Lines indicate mean. Data are normalized to cyclophillin. Each data point represents one lymph node from individual mice (n=6–8 mice/group from 3 separate experiments). **(k)** BAFF protein production in FRC-ablated mice was determined by confocal microscopy in lymph nodes from *Ccl19*-Cre x iDTR stained with an

antibody against BAFF together with DAPI. Scale bars 50 μm (n=2 mice from two separate experiments). ^{NS} non significant, *p<0.05, **p<0.01, ***p<0.001

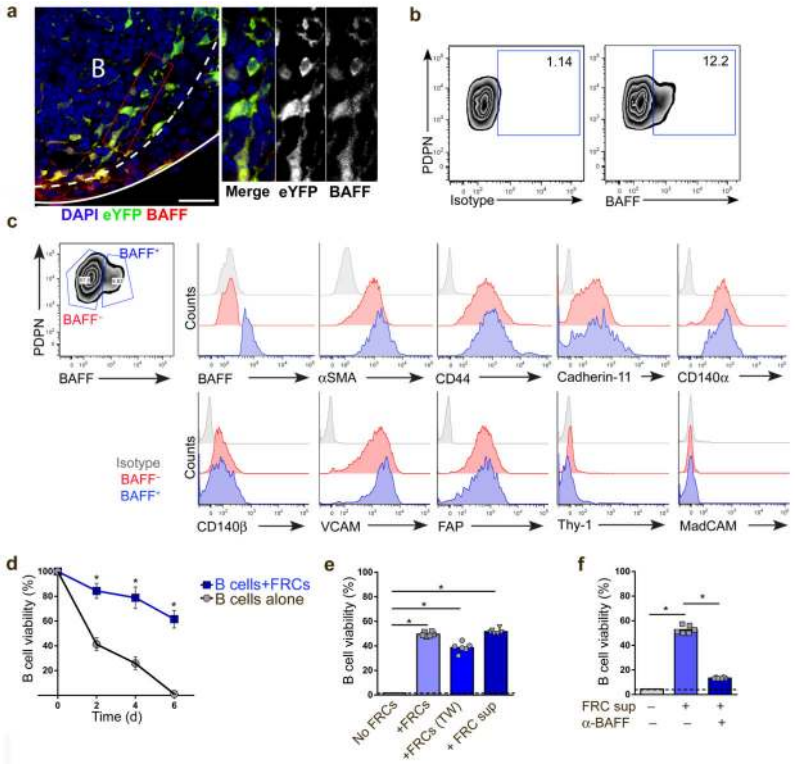

Figure 7. FRCs support the survival of B cells through the production of BAFF

(a) BAFF production by FRCs (EYFP$^+$ cells) was determined in *Ccl19*-Cre x *Rosa26*-EYFP mice by staining lymph nodes with a BAFF-specific antibody together with anti-GFP and DAPI. Line depicts lymph node capsule while dotted line delineates B cell follicle. Scale bar 20 μm (n=3 mice from two separate experiments). **(b)** BAFF production by FRCs (PI$^-$CD45$^-$PDPN$^+$CD31$^-$MadCAM$^-$ cells) was determined by flow cytometry in freshly isolated lymph node stromal cells. Numbers indicate percent (n>6 mice from 3 separate experiments). **(c)** Flow cytometric analysis of canonical FRC marker expression in BAFF$^+$ or BAFF$^-$ FRCs. **(d)** Purified B cells were cultured alone or in the presence of FRCs and cell viability was determined daily by enumerating the numbers of PI$^-$B220$^+$ cells in each well. Data represent three independent experiments (mean+/−sem, n=2–4 wells/group per experiment). **(e)** B cell viability was determined at day 5 in B cells cultured alone, in contact with FRCs, separated from FRCs by a transwell filter (TW), or with FRC-conditioned culture supernatant (FRC sup). Data represent three independent experiments (mean, n=2–4 wells/group per experiment). **(f)** B cells were cultured alone or with FRC-conditioned supernatant (FRC sup). BAFF-specific neutralizing antibody was added to some of the wells and B cell viability was determined by flow cytometry. Data represent three independent experiments (mean, n=2–4 wells/group per experiment). * p<0.001